Earthq Eng & Eng Vib (2021) 20: 687-704 **DOI**: https://doi.org/10.1007/s11803-021-2047-2

Substructure design optimization and nonlinear responses control analysis of the mega-sub controlled structural system (MSCSS) under earthquake action

Mustapha Abdulhadi†, Zhang Xun′an‡, Buqiao Fan† and Muhammad Moman†

College of Mechanics and Civil Engineering, Northwestern Polytechnic University, Xi'an 710071, China

Abstract: The newly proposed mega sub-controlled structure system (MSCSS) and related studies have drawn the attention of civil engineers for practice in improving the performance and enhancing the structural effectiveness of mega frame structures. However, there is still a need for improvement to its basic structural arrangement. In this project, an advanced, reasonable arrangement of mega sub-controlled structure models, composed of three mega stories with different numbers and arrangements of substructures, are designed to investigate the control performance of the models and obtain the optimal model configuration (model with minimum acceleration and displacement responses) under strong earthquake excitation. In addition, the dynamic parameters that affect the performance effectiveness of the optimal model of MSCSS are studied and discussed. The area of the relative stiffness ratio RD, with different mass ratio MR, within which the acceleration and displacement of the optimal model of MSCSS reaches its optimum (minimum) value is considered as an optimum region. It serves as a useful tool in practical engineering design. The study demonstrates that the proposed MSCSS configuration can efficiently control the displacement and acceleration of high rise buildings. In addition, some analytical guidelines are provided for selecting the control parameters of the structure.

Keywords: mega sub-controlled structure system (MSCSS); optimal model; viscous damper; dynamic parameters; control effectiveness; response control; rubber bearing

1 Introduction

As the availability of building construction sites is limited and demand is increasing globally, more attention is focused on designing tall and super tall buildings to address the economic challenges that have resulted from the rise in the cost of land. Some examples of these types of tall buildings are located in Hong Kong, Shanghai, and Tokyo.

The structural arrangement of these types of buildings is regarded as a mega-substructure (MSS), as shown in Fig. 1(a). The structure comprises a megastructure, which is its principal fundamental element, and many sub-frames, each composed of several floors utilized for business and residential purposes. In these types of structural arrangements, the substructures are stiffly attached to the mega-structure and could be designed into different indigenous forms as desired. In addition, mega-substructure configuration possesses a more robust capacity to withstand horizontal forces generated by wind and earthquakes. However, its structural safety under severe shock and heavy wind loads remain a significant concern in the design of these mega-substructures.

For the past decade, many types of research have been carried out to investigate traditional seismic response problems and developed a better configuration that will address these challenges and further ensure the structural integrity of mega-substructure under extreme earthquakes and strong winds. Among these are the work of Ndemanou *et al*. (2013) to use a magnetorheological fluid damper at a specified point of the beam to reduce the vibration of the structure subject to the earthquake. Benoit *et al.* (2013) showed that the finite element method (FEM) could be used to determine the dynamic behavior of the structure and precisely predict the vibration frequency. Khan *et al*. (2020) developed a mechanics based damaged scale for steel structures, to support simplify structural health monitoringand understanding of weak structural element. Murat *et al.* (2013) studied the performance of steel buildings and nonstructural elements during Chile′s earthquake in 2010, and the result showed that structural steel buildings performed well and sustained limited damage except for nonstructural parts. Amini and Doroudi (2010) used a fuzzy control technique to effectively control the seismic

Correspondence to: Mustapha Abdulhadi, Northwestern Polytechnical University, Xi′an 710071, China
Tel: +86-13109588448
E-mail: engineerabdulhadi2@yahoo.com
†PhD Candidate; ‡Professor;

Supported by: National Natural Science Foundation of China under Grant No. 51878274
Received November 1, 2019; **Accepted** December 14, 2020

response of the structure. The results show that semi control and hybrid semi control can efficiently mitigate the seismic response of the building. Kim and Lee (2010) revealed that the control performance of semi-active tuned mass damper (STMD) controlled by an optimal fuzzy controller is superior to that of the passive TMD. The studies conducted by Anwar and Dong (2020), Yang *et al.* (2020), Vona and Mastroberti (2018) prove that seismic resilience can serve as a performance tool to evaluate the continuing effects of a hazard for the retrofit selection.

Feng and Mita (1995) were the first to introduce the response control principle of high-rise skyscrapers subjected to severe shocks. The proposed structure exhibited an isolated substructure, which can be used to overcome the vibration of the whole building. The result revealed that the function of the substructure of this building behaved more like a tuned mass damper (TMD). Subsequently, Chai and Feng (1997) advanced this arrangement based on the control principle of the tuned mass damper (TMD) by presenting a passive mega sub-controlled structure (PMSCS). In this configuration, the authors used concentrated mass to represent the substructure and a cantilever beam as a megastructure. Furthermore, to improve this configuration, Lan *et al.* (2002) presented a multi-purpose mega-system established by a combination of a base-isolated substructure and a tuned mass damper (TMD).

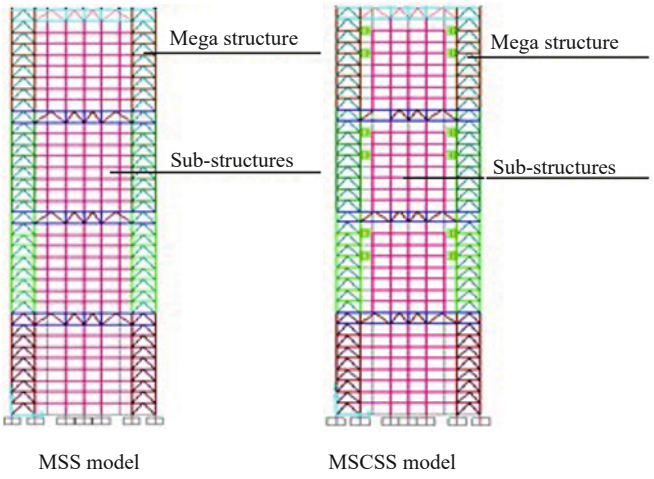

(a) Two schematic models (MSS and MSCSS)

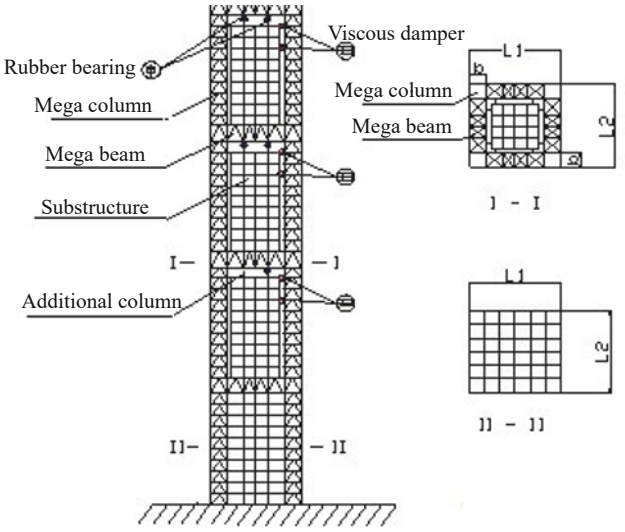

(b) Close-up view of the details MSCSS model

Fig. 1 Structural configuration of MSS and MSCSS

Recently, based on this structural configuration, an advanced structure called the mega sub-controlled structure system (MSCSS) was introduced (Zhang *et al.*, 2004). In this configuration, the authors designed the substructure as a modulated substructure and attached it to the mega beam; and introduced an additional column connecting the mega-structure and top level of the substructure to address the problem of a very long span of the mega beam and mega-beam story structure, as shown in Fig. 1(a). Later, Zhang *et al*. (2005a) used a similar simplified model to improve the effects of MSCSS using random wind loads and random earthquakes. In addition, the introduction of a friction damper into the substructure of an MSCSS further increased its wind and earthquake resistance capability much more than in the mega-substructure (Lian *et al*., 2007).

Later, Zhang *et al.* (2009) presented and discussed a parametric study of the structural characteristics as an active mechanism for regulating the vibration response of high rise mega-structures. In recent studies (Zhang *et al*., 2004, 2005a, 2005b, 2009; Abdulhadi *et al.*, 2020b; Fan *et al.*, 2020), different controlling principles were analyzed and compared to MSS. To further improve the control effectiveness of the system and enhance the mechanical performance of the additional column in MSCSS, Abdulhadi *et al.* (2020a) proposed additional improvements where rubber bearings are presented at the pick level of the additional column. This esearch showed that MSCSS increases structural safety under seismic action and decreases structural response under earthquake load. However, some difficulties still exist with its design that need to be improved before the proposed structure can be used in practice. Currently, experimental investigations of this type of structure remain insufficient due to the complexity of the structure and model uncertainty. Therefore, a full and comprehensive simulation analysis of the mega sub-controlled structure to examine the control characteristics of the model before an experimental investigation has remained necessary to the research world. In this study, using SAP 2000 finite element software, (Computer & Structure, Inc. 2014. V. 17), the influence of the different structural configurations of MSCSS on the seismic performance, and how to determine an optimal model to minimize the displacement and acceleration response are investigated. In addition, the impact of the dynamic parameters of mass, stiffness and damping properties of the subframes compared to those of the mega-structure

and how they affect the numerical results are studied to provide a source for experimental studies as well as practical guidelines for engineering designers.

2 Response control principle of MSCSS system

The configuration of MSCSS includes the mega-structure, substructure, and viscous damper comprise the fundamental elements of the modulated sub structural controlled system (see Fig. 1(b)). The substructures have frequency-modulated capacity and are referred to as a frequency modulated substructure. In this arrangement (substructures are contained within the mega-frame), the new controlling principle is established. Due to the dynamic behavior of the structure, the vibration energy generated from earthquake loads is transferred to the substructures. Then the transferred energy is dispersed within the substructure. These can be established by the optimum design of substructures and installing viscous dampers between the mega-frame substructures for energy dissipation. An additional column could be introduced at the top floor of the substructure to overcome the long span problem of the beam. The rubber bearing could also be designed at the top of the additional column to improve the structural design of MSCSS and further reduce the structural response.

The principle of the MSCSS configuration, where substructures themselves serve as vibration absorbers, uses the interaction between the mega-frame and substructure to suppress or control the building vibration. Sub-frames naturally have several vibration modes; therefore, the sub-frames can absorb energy in a broad frequency range. This control system presents an explicit load transmission. The mega-structure is the main lateral force and load-bearing system. At the same time, sub-frames play a supporting role and energy absorbers during an earthquake are responsible for the transfer of vertical loads to the mega-frame. Therefore, they offer an evident energy flow. In addition, the control system is cost-effective because it does not require any additional mass to perform its efficiency. Sub-frames, between the mega-structure, can act as the tuned mass stroke in the TMD system.

Although the basic principle of MSCSS is related to the concept of the tuned mass damper, it is distinct from the single superposition of the conventional mega-structural frame with a TMD system. The differences between these systems are explained as follows:

1. Substructures can be adjusted as needed on several mega-floors, and each substructure is designed as a multiple-degree-of-freedom system. This configuration is distinct from the TMD system.

2. The performance of the substructures of MSCSS changes when the structure reaches the elasto-plastic state; while the TMD system does not regard the elastoplastic disposition of the lumped mass structure.

This means that the concept of the MSCSS is more complicated, and some aspects are not listed but require study. Other than the MSCSS fundamental principle discussed above, some control systems such as active control, semi-active control and hybrid control can be efficiently implemented on an MSCSS configuration (Zhang *et al*., 2004) to further improve the structural response of the MSCSS model under seismic load. In addition, it is straightforward to install an actuator or magnetorheological damper (MRD); or the actuator combined with a viscous damper between the mega-frame and the substructure. In this study, the aim is not only to improve the response of the mega-structure but also reduce the vibration response of the substructure under a strong earthquake. It is necessary, therefore, to investigate the effect of different structural configurations of MSCSS to determine an optimal model to minimize the displacement and acceleration response, as well as to study the dynamic parameters of mass, stiffness and damping properties of the subframes compared to those of the mega-structure and how they affect the numerical results.

3 Analytical lumped mass model of mega-sub controlled structure and dynamic equation

The MSCSS configuration is presented in Fig. 2, where the structure is composed of the mega-structure, which is the main building frame and many sub-frames attached to the mega-frame. Each sub-frame contains many stories used for business or residential purposes. For this type of structure, where the bending is considered as the predominant vibration mode, the mega-frame should be modelled as a cantilever beam. This cantilever beam is further discretized as a multi-degree-of-freedom (MDOF) system, and it seems that a shear-type structural model can be appropriate for a sub-structure. As mentioned before, the proposed mega sub-controlled structure should have a mutually collaborating substructure, so that the synergy between the mega-frame and the substructure can be utilized to mitigate the structural vibration. Since the sub-frames are usually not slender, the shearing is the governing mode and is also treated as a MDOF system. The substructure

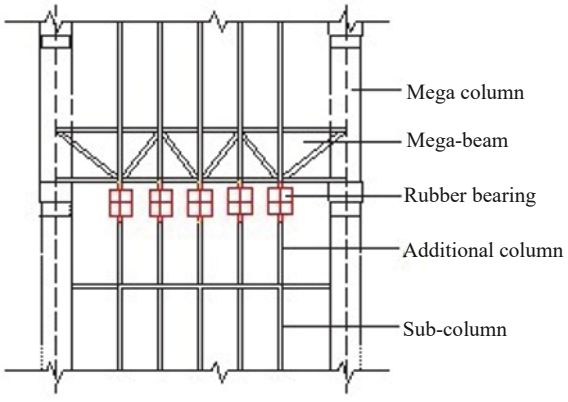

Fig. 2 Additional column with rubber bearing in MSCSS Configuration

is composed of a modulated substructure and attached to the mega-beam structure and, unlike the configuration of the substructure originally introduced by Chai and Feng (1997), some extra columns are added between the mega-beam floor and the peak level of the substructure to improve the over-large span of the structure. In addition, a lead rubber bearing is designed at the peak of the additional column to relax the horizontal constraints between the mega-beam floor and the additional column and further reduced the sub-structural responses and the entire structure as shown in Fig. 2. Two viscous dampers are also installed at each of the 2nd, 3rd and 4th mega-floors.

For the analytical lumped mass model, each story is assumed as a single concentrated mass. The structure is discretized into a set of lumped masses, each having a weight equal to the sum of the weight of a mega-frame and substructure′s masses. Therefore, the analytical model of the MSCSS configuration can be obtained, as shown in Fig. 3(b) and that of the conventional MSS is presented in Fig. 3(a).

From Fig. 3(b), let the configuration possess n mega stories and n_s sub-frames, each consisting of n_z floors relative to the mega-frames, the mass damping, and shear stiffness will then have the sum of $n + n_s \times n_z = N$ degree of movement. An equation governing the motion of this structure is expressed below:

$$\boldsymbol{M}\ddot{\boldsymbol{u}}(t) + \boldsymbol{C}\dot{\boldsymbol{u}}(t) + \boldsymbol{K}\boldsymbol{u}(t) + \boldsymbol{p}(t) = \boldsymbol{F}(t) \tag{1}$$

where the vector $\boldsymbol{u} = \left[u_{\mathrm{P}}{}^{\mathrm{T}},\ u_1{}^{\mathrm{T}},\ u_2{}^{\mathrm{T}} \ldots\ u_{ni}{}^{\mathrm{T}}\right]^{\mathrm{T}}$ represents the displacement vector of the system having $n + n_s \times n_z$ variables. $\boldsymbol{u}_{\mathrm{P}}{}^{\mathrm{T}}$ and $\boldsymbol{u}_i{}^{\mathrm{T}}\left(i = 1,2,\ldots.,n_i\right)$ are the displacement vectors of the mega-structure and ith substructure. $\boldsymbol{M}$, $\boldsymbol{C}$, and $\boldsymbol{K}$ represent the global mass, damping and stiffness matrix, respectively, and $\boldsymbol{F}$ represents the applied force of the structure (Zhang *et al.*, 2005a).

$\ddot{\boldsymbol{u}}(t)$ — Velocity

$\dot{\boldsymbol{u}}(t)$ — Acceleration

$\boldsymbol{M}$ describes the mass matrix, as shown below:

$$\boldsymbol{M} = \mathrm{diag}\left[\boldsymbol{M}_{\mathrm{P}}, \boldsymbol{M}_1, \boldsymbol{M}_2, \boldsymbol{M}_3, \ldots\ldots\boldsymbol{M}_i, \ldots\ldots, \boldsymbol{M}_{ns}\right] \tag{2}$$

where $\boldsymbol{M}_{\mathrm{P}} = n \times n$ diagonal mass matrix of the mega-frame, and $\boldsymbol{M}_i (i = 1,2,3\ldots..,n_{\mathrm{S}}) = n_z \times n_z$ mass matrix of the ith sub-frame.

While the stiffness matrix $\boldsymbol{K}$ is presented as:

$$\boldsymbol{K} = \begin{pmatrix} \boldsymbol{K}_{\mathrm{P}} + \boldsymbol{K}_{\mathrm{s,diag}} & \boldsymbol{K}_{\mathrm{c}} \\ \boldsymbol{K}_{\mathrm{c}}{}^{\mathrm{T}} & \boldsymbol{K}_{\mathrm{s}} \end{pmatrix} \tag{3}$$

$$\boldsymbol{K}_{\mathrm{s}} = \mathrm{diag}\left[\boldsymbol{K}_{\mathrm{s},1}, \boldsymbol{K}_{\mathrm{s},2}, \boldsymbol{K}_{\mathrm{s},3}, \ldots\ldots, \boldsymbol{K}_{\mathrm{s},i}, \ldots\ldots, \boldsymbol{K}_{\mathrm{s},ns}\right] \tag{4}$$

where $\boldsymbol{K}_{\mathrm{P}} = n \times n$ stiffness matrix is related to the mega-structure; $\boldsymbol{K}_{\mathrm{s},i} (i = 1,2,3\ldots..,n_{\mathrm{S}}) = n_z \times n_z$ is the stiffness matrix related to the ith sub-structure.

$\boldsymbol{K}_{\mathrm{c}}$ is the coupling item between the mega-structure and the sub-structures and has $n \times n_1 n_z$ matrix elements.

The damping matrix is obtained as follows:

$$\boldsymbol{C} = \begin{pmatrix} \boldsymbol{C}_{\mathrm{P}} + \boldsymbol{C}_{\mathrm{s,diag}} & \boldsymbol{C}_{\mathrm{c}} \\ \boldsymbol{C}_{\mathrm{c}}{}^{\mathrm{T}} & \boldsymbol{C}_{\mathrm{s}} \end{pmatrix} \tag{5}$$

$$\boldsymbol{C}_{\mathrm{s}} = \mathrm{diag}\left[\boldsymbol{C}_{\mathrm{s},1}, \boldsymbol{C}_{\mathrm{s},2}, \boldsymbol{C}_{\mathrm{s},3}, \ldots\ldots, \boldsymbol{C}_{\mathrm{s},i}, \ldots\ldots, \boldsymbol{C}_{\mathrm{s},ns}\right] \tag{6}$$

where $\boldsymbol{C}_{\mathrm{P}} = n \times n$ is the damping matrix related to the

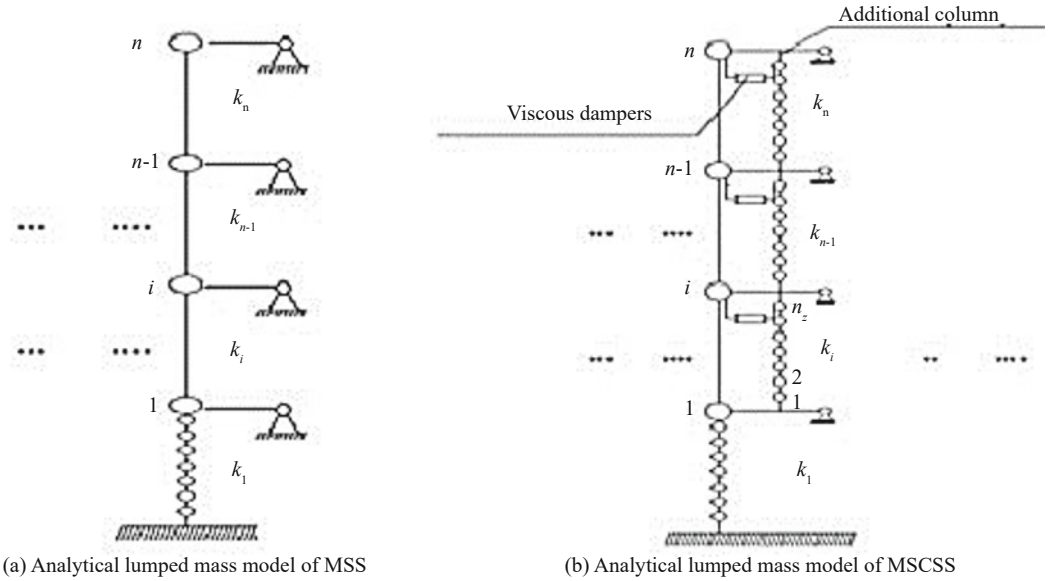

(a) Analytical lumped mass model of MSS (b) Analytical lumped mass model of MSCSS

Fig. 3 Analytical lumped mass of MSS and MSCSS models

mega-structure and $\boldsymbol{C}_{s,i}(i=1,2,3.....,n_S)=n_z\times n_z$ is the damping matrix of the *i*th sub-structure.

$\boldsymbol{C}_c$ is the $n\times n_s n_z$ coupling damping matrix between the mega-structure and sub-structures.

In addition, $\boldsymbol{p}(t)$ from Eq. (1) represents the load vector provided by the viscous dampers and rubber bearings. Therefore, $\boldsymbol{p}(t)=\boldsymbol{p}_d(t)+\boldsymbol{p}_{rb}(t)$. Where $\boldsymbol{p}_d(t)$, is the force in the damper and $\boldsymbol{p}_{rb}(t)$ represent the force in the rubber bearings.

4 Numerical analysis of MSCSS

According to the Chinese code of design, two natural earthquake records and one artificial wave must be considered for the design of any structural system (GB 50011-2010, 2010). Elghazoul (2002) used El Centro and Taft waves explicitly because they are often employed for analysis of the mega-system.

In this study, two natural waves, Taft-NE wave and El Centro, 1940-NS, records, and two artificial earthquake records are used to examine the control effectiveness of this structure. The artificial wave adopted in this research depends on the Hilbert Huang transform (HHT) approach. All the input seismic energy waves are analyzed in a period of the first 50 seconds under 10 Hz. The peak ground acceleration (PGA) is scaled to 0.4 g. Because the GB50011 (2010) allows some structural members to be plastically deformed during earthquakes, dampers and rubber bearings in the proposed MSCSS are also nonlinear; therefore, nonlinear dynamic analysis is adopted. In this study, the simulation result is determined by the nonlinear direct integration time history analysis (NTHA) method, as presented in the subsequent sections.

4.1 Hilbert – huang transform (HHT)

Norden E. Huang introduced an alternative analytical mechanism named the Hilbert – Huang transform (HHT) (Gabor, 1946). The HHT approach for examining data consists of two components: Hilbert spectral analysis, which is a spectral analysis tool, and empirical mode decomposition (EMD).

4.1.1 Hilbert spectral analysis

HHT provides a different technique to introduce spectral analytical mechanisms to deliver time-frequency–energy details of the time series data. For an irrational function $x(t)$ of the LP form, its Hilbert transform, $y(t)$, is given by Eq. (7) (Byron and Fuller, 1992).

$$y(t)=\frac{1}{\pi}PV\int_{-\infty}^{\infty}\frac{\ddot{x}(\tau)}{t-\tau}\mathrm{d}\tau \tag{7}$$

where PV represents Cauchy′s principal value integral, Byron and Fuller (1992) suggested that the Hilbert transform pair can be used to form an analytic function, as displayed in Eq. (8).

$$Z(t)=x(t)+\mathrm{i}y(t)=A(t)\mathrm{e}^{\mathrm{i}\theta(t)} \tag{8}$$

where $A(t)=(x^2+y^2)^{1/2}$, $\theta(t)=\tan^{(-1)}\left(\frac{y}{x}\right)$, and $\mathrm{i}=\sqrt{-1}$.

$A(t)$ and $\theta(t)$ denote the amplitude and phase function, sequentially (Byron and Fuller, 1992). The frequency is derived from the time derivatives of the phase, as displayed in Eq. (9).

$$f=\frac{\delta\theta}{\delta t}(t) \tag{9}$$

Since the frequency function and the amplitude are expressed as the function of time, then a marginal specimen can be written as in Eq. (10).

$$E(w)=\int_0^T H(f,t)\mathrm{d}t \tag{10}$$

4.1.2 Empirical mode decomposition (EMD)

EMD is an algorithm used to break down almost every signal into many functions. These functions are referred to as intrinsic mode functions (IMFS). The process involves an iterative sifting process as described below:

- Find the local maxima and minima of the signal.
- Create an upper envelope about the signal by linking the maxima with an interpolation function.
- Create a lower envelope about the signal by linking the minima with an interpolation function.
- Calculate the half of the difference within the upper and the lower envelope as the local mean.
- Deduct the local mean from the signal and repeat the process.

The procedure is repeated until the signal has a zero mean and the number of extrema (maxima and minima) and zero-crossing varies by at most one (Gabor, 1946). Then, the difference between IMF and the original signal is noted, and the procedure is repeated on the remainder. This process is repeated until the final residue is a monotonic function. Equation (11) represents the signal $D(t)$ after the signal has been fully decomposing.

$$D(t)=R_n(t)+\sum_{j=1}^{n}IMF_j(t) \tag{11}$$

where $R_n(t)$ represent the final residue.

From Eq. (10) and Eq. (11), the analytical function can be expressed as:

$$D(t)-R_n(t)=R_e\left[\sum\nolimits_{j=1}^{n}A_j(t)\mathrm{e}^{(\mathrm{i}sfj(t))\delta t}\right] \tag{12}$$

5 Substructure design optimization of MSCSS model

As mentioned earlier, MSCSS is formed by rebuilding a conventional mega-substructure in such a way that the substructure is relatively isolated and can effectively suppress the vibration of the etire structure. The configuration proposed herein consists of four mega-floors, with the first mega-floor having an attached substructure and a 2nd, 3rd and 4th with a modulated substructure. The main objectives of the optimization at this point, are to find the optimal number, position and arrangement of the substructure within the mega-frame so that the response of the entire structure can be improved.

To achieve this, five different models are designed and investigated, as shown in Fig. 4. The model with a minimum target response (displacement and acceleration) is regarded as an optimal design model and used to examine the dynamic parameters of the models. Various optimal distribution strategies exist in the literature that are based not only on displacement and acceleration minimization but also and most importantly, on energy concepts. For example, a non-repetitive method is employed in comparison with the SSSA method for distributing a damping coefficient of the viscous damper along with the building height (Hwang *et al.*, 2013). Zhou and Tan (2018) present design rules and some novel and innovative strategies for seismic isolation and energy dissipation for building and civil engineering structures. An energy-based stochastic approach is employed by integrating novel equal energy non-Gaussian SLT in the optimal design (De Domenico and Ricciardi, 2019b). Whittle *et al.* (2012) studied and compared the usefulness of two standards and three advanced viscous dampers placement methods based on

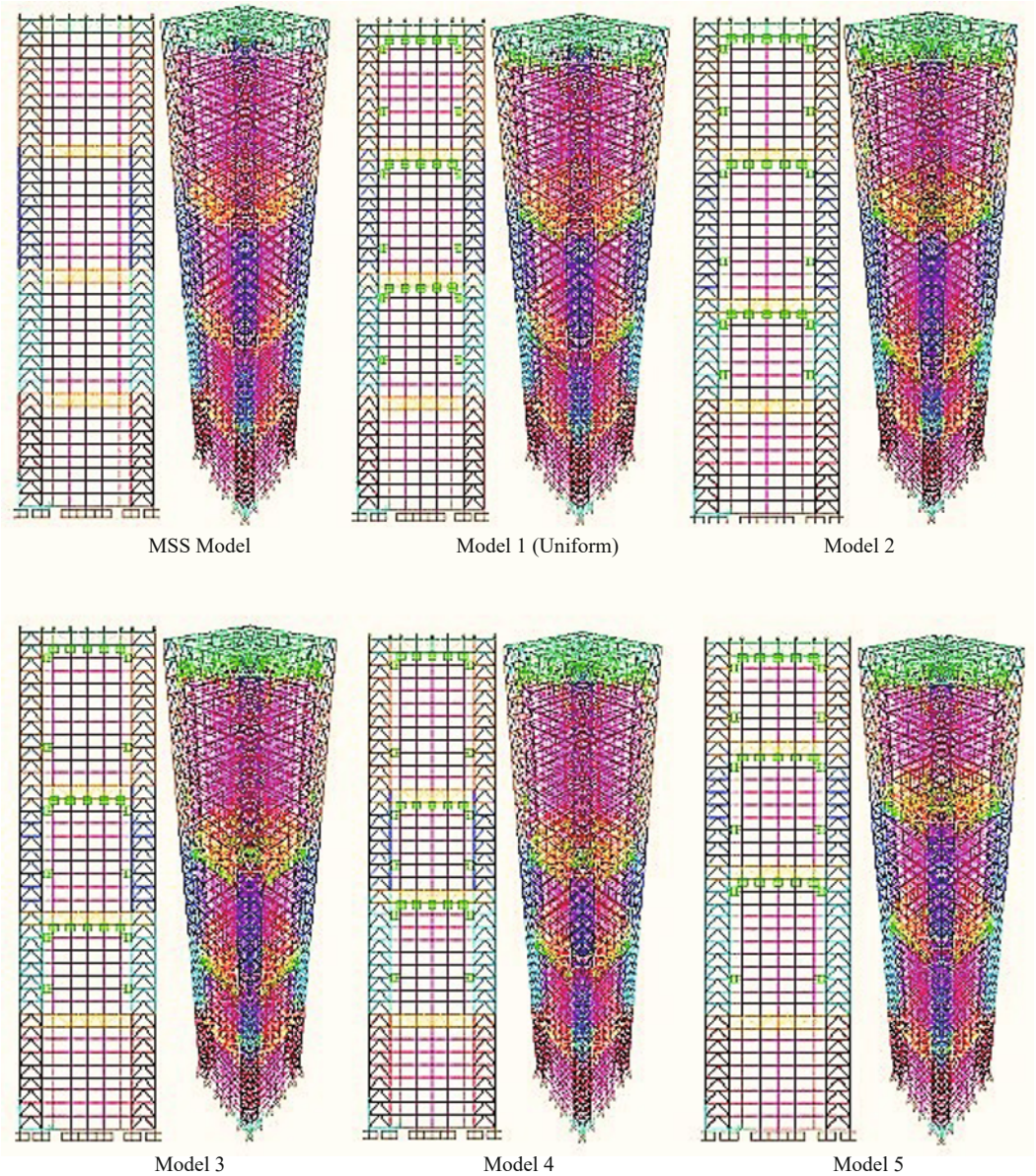

Fig. 4 2D and 3D Models of MSS and MSCSS with different numbers and arrangements of substructures

Table 1 Section properties of the member

Members	Member sections	Area	Moment of inertia		Section modulus		Radius of gyration	
	($\times 10^{-3}$ m)	($\times 10^{-4}$ m^2)	I_x ($\times 10^{-9}$ m^4)	I_y ($\times 10^{-9}$ m^4)	W_x ($\times 10^{-6}$ m^3)	W_y ($\times 10^{-6}$ m^3)	R_{gx} ($\times 10^{-3}$ m)	R_{gy} ($\times 10^{-3}$ m)
Mega-column member in first mega structural floor	□600 × 600 × 60 × 60	1,296	6,376,000	6,376,000	21,300	21,300	221.8	221.8
Mega-column member in second mega structural floor	□600 × 600 × 60 × 60	1,296	6,376,000	6,376,000	21,300	21,300	221.8	221.8
Mega-column member in third mega structural floor	□600 × 600 × 40 × 40	896	4,707,000	4,707,000	15,700	15,700	229.2	229.2
Mega-column member in fourth mega structural floor	□600 × 600 × 20 × 20	464	2,605,000	2,605,000	8,680	8,680	236.9	236.9
Mega-beam member (Floor 8 – 9)	**H**1000 × 350 × 25 × 16	327	5,303,000	179,000	10,600	1,023	402.7	74
Mega-beam member (Floor 18 – 19)	**H**1000 × 350 × 25 × 16	327	5,303,000	179,000	10,600	1,023	402.7	74
Mega-beam member (Floor 28 – 29)	**H**1000 × 350 × 25 × 16	327	5,303,000	179,000	10,600	1,023	402.7	74
Mega-beam member (Floor 38 – 39)	**H**1000 × 350 × 25 × 16	327	5,303,000	179,000	10,600	1,023	402.1	74
Mega-column web member (For 1st mega floor)	**H**350 × 300 × 25 × 25	225	453,100	112,900	2,589	752.6	141.9	70.8
Mega-column web member (For 2nd - 4th mega floor)	**H**350 × 300 × 19 × 12	151	343,000	85,540	1,900	570.3	150.5	75.2
Mega-beam web member (For 1st – 3rd mega floor)	**H**350 × 300 × 20 × 19	179	374,300	90,180	2,139	601.2	144.6	71
Mega-beam web member (For 4th mega floor)	**H**350 × 350 × 19 × 12	170	395,100	135,800	2,257	776.1	152.2	89.3
Sub-column member	□430 × 430 × 10 × 10	83	174,500	26,070	997.1	208.6	145	56
Sub-beam member	**H**350 × 250 × 10 × 10	168	494,200	494,200	2,299	2,299	171.5	171.5
Additional column member	□430 × 430 × 10 × 10	83	174,500	26,070	997.1	208.6	145	171.5

the reduction of absolute acceleration, peak inter-story drift, and residual drift. De Domenico *et al.* (2019b) presented some energy-based techniques to interpret the seismic performance in terms of the energy dissipated by the fluid viscous dampers from the earthquake excitation.

The models are designed as described below:

Model 1 consists of four mega-floors, with a uniform number and arrangement of a "modulated substructure" (eight stories) throughout the mega-floors.

Model 2 consists of eight stories of "attached substructures" at the bottom (the 1st mega-floor) and six, ten and eight "modulated substructures" at the 2nd, 3rd and 4th mega-floor structure, respectively.

Model 3 consists of eight "attached substructures" at the bottom; and six, eight and ten "modulated substructures" on the 2nd, 3rd, and last mega-floor structure, respectively.

Model 4 is composed of eight "attached substructures" at the 1st mega-floor, eight "modulated substructures" at the 2nd mega-floor and six and ten "modulated substructures" at the 3rd and 4th mega-floor structure, respectively.

Model 5 consists of eight attached substructures at the bottom and ten, eight and six "modulated substructures" at the 2nd, 3rd, and 4th mega-floor structure, respectively.

The above models consist of two viscous dampers installed between the mega-frame and sub-frame of each 2nd, 3rd and 4th mega floor and a rubber bearing designed at the top of the additional column. To reasonably evaluate the performance of these models, the same parameters of viscous dampers and rubber bearings are used for all of them, and are adopted as per Section 5.3 and Table 2, respectively, in (Abdulhadi *et al*., 2020a).

In this study, the fast nonlinear analysis (FNA) method using eigenvectors is employed to obtain the target responses, which are the displacement and acceleration of the buildings. Analyzing the above models with the same parameters of viscous damper and rubber bearing, using the El Centro 1940 (NS) wave with a peak velocity of 25 cm/s, the maximum target responses (displacement and acceleration) values can be obtained for different building models. The peak ground acceleration is set at 0.4 g, and the analysis result is plotted in Figs. 5–6. Here, the maximum response value of displacement and acceleration along the structural floors is chosen as the target response and compared to those of the conventional megastructure (MSS). The model that generates minimum target responses is considered as the optimally designed model for use in further studies.

The analysis results from Figs. 5–6 show that the target responses of Model 3, Model 4 and Model 5 are significantly reduced as compared to Model 1, Model 2 and the MSS Model. The reduction in the vibration responses of these buildings clearly shows the influence of the substructural arrangement, especially at the top of the building. The results summarized in Tables 1 and 2 show that the acceleration and displacement of Model 4 (with eight, six and ten substructure arrangements, respectively) are significantly reduced. In addition, Figs. 5 and 6 reveal that minimum acceleration and displacement responses are obtained when the building is composed of a lesser number of substructures in the middle (the 3rd mega-floor) of the structure. However, it is challenging to obtain minimum target responses of the building at the top and bottom simultaneously (model 5). As seen from the results, Model 4 achieved this requirement better and is considered as an optimal design model for use in more investigations.

6 Expression of displacement and acceleration responses of MSCSS

6.1 Complex model analytical method

From Eq. (1), matrix $\boldsymbol{C}$ expressed by Eq. (5) with the added damper effects cannot be uncoupled due to its unproportioned pattern. However, it has been recently demonstrated that the modal mass ratio alone is not sufficient to ascertain the accuracy of a truncated model. A measure that is related to the damping matrix called the modal dissipation ratio of each mode in a complex modal analysis framework should be considered when constructing a reduced-order model (De Domenico

Table 2 Acceleration and displacement response at a critical point of the structure under the El Centro wave

	Mega Structure top Floor		4th Substructure top Floor		3rd Substructure top Floor		2nd Substructure top Floor	
	Accel. (m/s^2)	Displ. ($\times10^{-2}$ m)	Accel. (m/s^2)	Displ. ($\times10^{-2}$ m)	Accel. (m/s^2)	Displ. ($\times10^{-2}$ m)	Accel. (m/s^2)	Displ. ($\times10^{-2}$ m)
MSS	14.74	7.80	12.70	4.93	11.72	4.73	10.23	5.10
MODEL 1	7.02 (52%)	7.00 (11%)	8.40 (34%)	4.32 (14%)	9.60 (18%)	4.31 (10%)	8.02 (22%)	2.90 (76%)
MODEL 2	7.50 (49%)	6.20 (26%)	8.60 (32%)	4.65 (6%)	9.40 (20%)	4.57 (4%)	7.50 (27%)	4.46 (14%)
MODEL 3	5.14 (65%)	7.30 (7%)	7.50 (41%)	4.64 (6%)	8.80 (25%)	4.55 (4%)	7.01 (31%)	4.44 (15%)
MODEL 4	5.09 (65%)	5.50 (42%)	4.50 (65%)	4.31 (14%)	6.50 (45%)	4.32 (9%)	5.00 (51%)	4.44 (15%)
MODEL 5	4.43 (70%)	6.50 (20%)	7.00 (45%)	4.35 (13%)	8.20 (30%)	4.55 (4%)	9.62 (6%)	4.30 (19%)

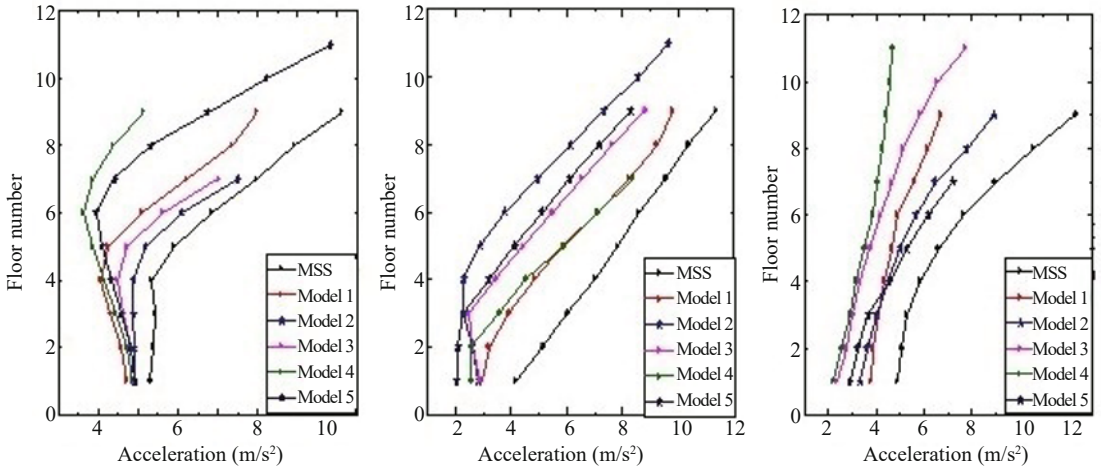

(a) 2nd mega-floor structure (b) 3rd mega-floor structure (c) 4th mega-floor structure

Fig. 5 Acceleration responses along with the mega sub-structural floor number

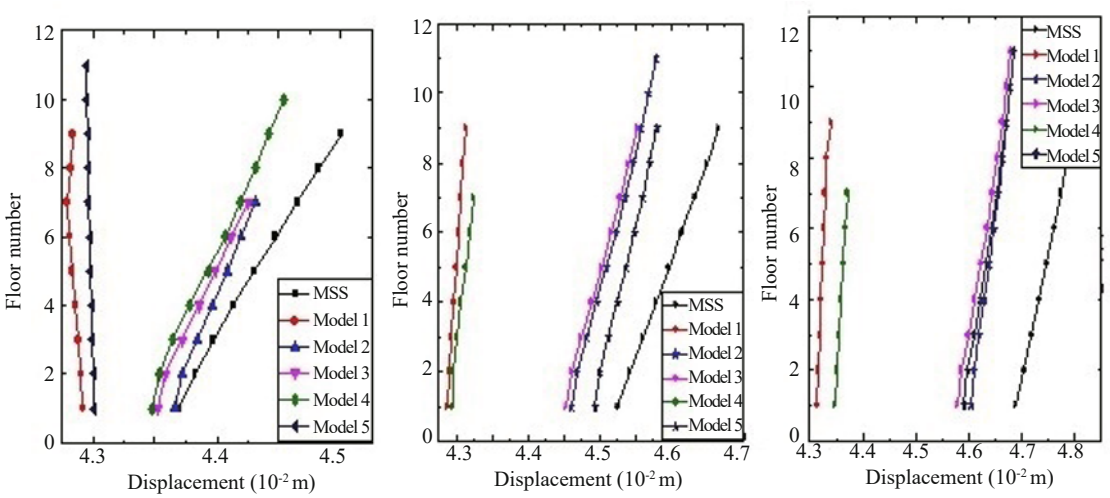

(a) 2nd mega-floor structure (b) 3rd mega-floor structure (c) 4th mega-floor structure

Fig. 6 Displacement responses along with the mega sub-structural floor number

and Ricciardi, 2019). It is, therefore, essential to use a complex model analytical method to decouple and find its solution.

After introducing a state vector, $\boldsymbol{r} = [\dot{X}^{\mathrm{T}}, X^{\mathrm{T}}]^{\mathrm{T}}$ into Eq. (1), the dynamic equation can be expressed as:

$$\boldsymbol{M}_r\dot{\boldsymbol{r}} + \boldsymbol{K}_r = \begin{Bmatrix} \boldsymbol{0} \\ \boldsymbol{f}(t) \end{Bmatrix} \tag{13}$$

where $\boldsymbol{M}_r$ is the mass matrix, and $\boldsymbol{K}_r$ is the stiffness matrix in the state space, as shown below:

$$\boldsymbol{M}_r = \begin{pmatrix} \boldsymbol{0} & \boldsymbol{M} \\ \boldsymbol{M} & \boldsymbol{C} \end{pmatrix} \quad \boldsymbol{K}_r = \begin{pmatrix} -\boldsymbol{M} & \boldsymbol{0} \\ \boldsymbol{0} & \boldsymbol{K} \end{pmatrix} \tag{14}$$

By further employing complex model transformation principles and considering the orthogonality of the model matrices, the decoupled dynamic equation can be written as:

$$\dot{Z}_i - P_i \times Z_i = m_i^{*-1} v_i^{\mathrm{T}} F(t),\ i = 1,\ 2,\ 3,\ldots\ldots,2N \tag{15}$$

where Z_i and P_i $(i = 1, 2, 3, \ldots\ldots, 2N)$, and $N = n + n_{\mathrm{s}} \times n_z$ are the model coordinate and system eigenvalues, respectively, v_i and u_i are the corresponding system left and right eigenvectors, respectively, and

$$m_i^* = v_i^{\mathrm{T}}\left[2PM + C\right] \cdot u_i \tag{16}$$

Using Duhamel integration, Eq. (15) can be written as:

$$Z_i(t) = \int_{-\infty}^{\infty} h_i(t-\mu) m_i^{i-1} v_i^{\mathrm{T}} F(\mu)\mathrm{d}\mu$$
$$i = 1,\ 2,\ 3,\ldots\ldots,2N \tag{17}$$

In addition, the cross variance function of $Z_i(t)$ and $Z_j(t)$ can be found.

6.2 Power spectral density of MSCS system

6.2.1 Expression of displacement and acceleration to stationary seismic excitation

In this case, the power spectral density (PSD) for the displacement $\boldsymbol{u}$ from Eq. (1) is expressed as:

$$S_x(f) = \boldsymbol{u} \cdot H(-f) \cdot \boldsymbol{B} \cdot S_n(f) \cdot \hat{H}(-f)^{\mathrm{T}} \cdot \bar{\boldsymbol{u}}^{\mathrm{T}}, \quad (18)$$

where $\boldsymbol{u} = [u_1\, u_2 \ldots\ldots u_{2N}]$, $H(-f)$ and $\hat{H}(-f)$ are the frequency function of $(-f)$ and conjugate frequency function of $(-f)$, respectively. $\boldsymbol{B}$ represents the coefficient matrix whose components are expressed by Eq. (19), and $S_n(w)$ is the PSD of acceleration excited at the base of the structure (Zhang *et al*., 2005):

$$b_{ij} = (m_i^*)^{\mathrm{T}} v_i^{\mathrm{T}} \Gamma \Gamma^{\mathrm{T}} \bar{v}_{(j)} \cdot \mathrm{conj}(m_j^*)^{(-\mathrm{T})} \quad (19)$$

The power spectral density (PSD) of the acceleration may be obtained from

$$S_{\ddot{X}}(f) = f^4 S_x(f) \quad (20)$$

Therefore, for stationary seismic excitation, the response values of the displacement and acceleration mean square are:

$$\delta_x^2 = \int_{-\infty}^{\infty} S_X(f)\mathrm{d}f \quad (21)$$

$$\delta_{\ddot{X}}^2 = \int_{-\infty}^{\infty} S_{\ddot{X}}(f)\mathrm{d}f \quad (22)$$

6.2.2 Expression of displacement and acceleration to non-stationary seismic excitation

Unlike stationary excitation, in this case, the structural power spectral density of the displacement and acceleration is the function of time (t) and frequency (f). The PSD of the displacement is described as:

$$S_x(t,f) = \boldsymbol{u} \cdot S_z(t,f) \cdot \bar{\boldsymbol{u}}^{\mathrm{T}} \quad (23)$$

where $S_z(t,f)$ is the complex model PSD response coordinate Z_i whose components $S_{z_{i,j}}(t,f)$ are described in the following form:

$$S_{z_{i,j}}(t,f) = b_{i,j} I_i(t,f) \bar{I}_i(t,f) S_n(f) \quad (24)$$

where $b_{i,j}$ represent the component of the coefficient matrices described by Eq. (13) and $I_i(t,f)$ is expressed as:

$$I_i(t,f) = \int_0^t h_i(t-\eta) A(t) \exp(-jfn)\mathrm{d}\eta \quad (25)$$

where h_i represents the complex coordinate of the impulse response function. In this case, $A(t)$ is described by a "Shinozuka–Sato" modulating function, expressed as:

$$A(t) = C_{\mathrm{sh}}[\exp(-\beta, t) - \exp(\beta_2 t)]$$
$$t \geq 0,\ \beta_1, \beta_2 > 0,\ \beta_1 < \beta_2 \quad (26)$$

where C_{sh} is the magnitude parameters of the modulating function, and β_1, β_2 are two exponential parameters of the function. Based on this expression for $A(t)$ in Eq. (26), Eq. (25) can be written as:

$$I_i(t,f) = \mathrm{e}^{pi} \left\{ \begin{array}{l} \dfrac{1}{-(P_{(i)} + \beta_1 + jf)} \left[\mathrm{e}^{-(P_i + \beta_1 + jf)t} - 1 \right] \\ + \dfrac{1}{P_i + \beta_2 + jf} \left[\mathrm{e}^{-(P_i + \beta_2 + jf)t} - 1 \right] \end{array} \right\} \quad (27)$$

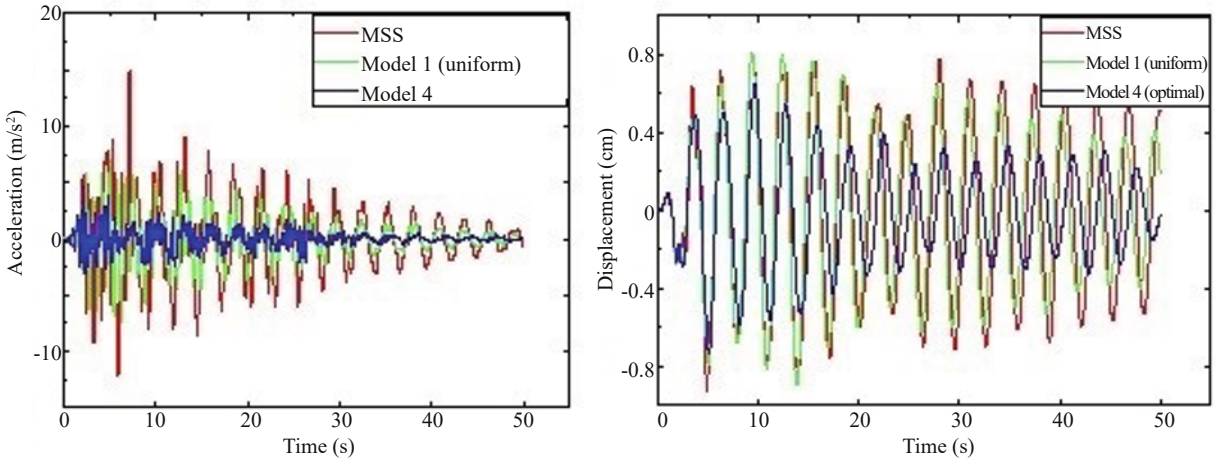

Fig. 7 Acceleration and displacement time history of the top structural mega floor

Although Eq. (21) and Eq. (22) can be used to calculate the mean square values of the displacement and acceleration, δx^2 and $\delta \ddot{x}^2$ respectively, Eq. (23) is invalid for calculating the PSD of the acceleration associated with non-stationary excitation. As such, the following procedure should be applied:

After determining the cross variance function of Z_i and $\dot{Z}_j$ and its Fourier transformation from Eq. (9) $\dot{Z}_i = m_i^{*-1} v_i^{\mathrm{T}} F(t) + P_i \cdot Z_i$, the PSD of the velocity correspondent $\dot{Z}$ can be expressed as:

$$S\dot{Z}_{i,j}(t,f) = b_{i,j} \cdot A_{(t)}{}^2 \cdot S_n(f) + P_i \cdot S_{z_{i,j}}(t\ f) \cdot \dot{P}_j + P_i \cdot b_{i,j} \cdot I_i(t,f) \cdot S_n(f) \cdot A(t) + b_{i,j} \cdot \bar{I}_j(t,f) \cdot A(t) \cdot \dot{P}_j \tag{28}$$

Then, the PSD $S_{\ddot{X}}(f)$ of the acceleration $(\ddot{X})$ and the acceleration mean square value $\delta_{\ddot{X}}^2$ can be calculated based on the transformation correlation between the complex coordinate and the space vector. As shown by Eq. (29) and Eq. (30):

$$S_{\ddot{X}}(f) = \boldsymbol{u} P[\dot{Z}_i \dot{Z}_j(f)] \dot{P}^{\mathrm{T}} \bar{\boldsymbol{u}}^{\mathrm{T}} \tag{29}$$

$$\delta_{\ddot{X}}^2 = \int_{-\infty}^{\infty} S_{\ddot{X}}(f) \mathrm{d}f \tag{30}$$

7 Optimum parameters investigation on the MSCSs

To effectively study the effectiveness of MSCSS under a strong earthquake due to its complex controlling mechanism, some parameters are considered. The megastructure and substructure mass ratio (*RM*), structural stiffness ratio (*RD*) and damping ratio (*RC*) are investigated, and the value which produces minimum target responses is considered as the optimal structural parameter value of the building. The influence of the three parameters is examined on the effectiveness of the building using Model 4 (the optimal model).

7.1 Sub and mega-structural mass ratio (*RM*)

The sub-structural vibrations in the mega sub-controlled structure system play the role of tuned mass or behave more like tuned mass in the tuned mass damper system. They must be carefully designed and controlled to a certain level to optimize the structure and enhance the safety of the residents and vibration-sensitive facilities. In this section, the proposed configuration (optimal model) is simulated using the two natural ground motions input (El Centro 1940 – NS and Taft NE) and two artificial waves (EI2 and RGB 3) scaled at 0.4 g. The impact of mass ratio on the proposed mega substructure and the optimal mass ratio value to suppress the vibration of the structure are investigated. In addition, the relative mass ratio (*RM*) between the substructure and the megastructure is investigated. The relative mass ratio (*RM*) is examined and defined by Eq. (31) as follows:

$$RM = \frac{\sum M_{\mathrm{sub}}}{\sum M_{\mathrm{mega}}} \tag{31}$$

where M_{sub} denotes the sub-structural mass and M_{mega} represents the mega-structural mass.

The results plotted in Figs. 8 and 9 show the influence of the mass ratio among the megastructure and substructure regarding the effectiveness of MSCSS. The figures display displacement and acceleration values at the peak of the mega structural floor using different mass ratio values. As observed from the figures, the acceleration and displacement values decrease as the mass ratio increases. This means that the control effectiveness of this structure will be better when the

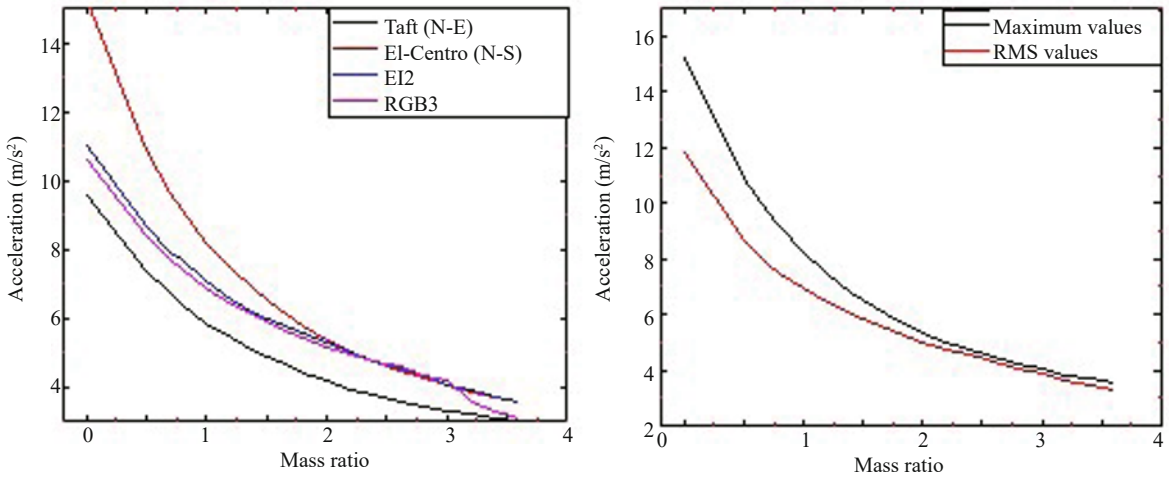

Fig. 8 Impact of mass ratio on the acceleration response of MSCSS

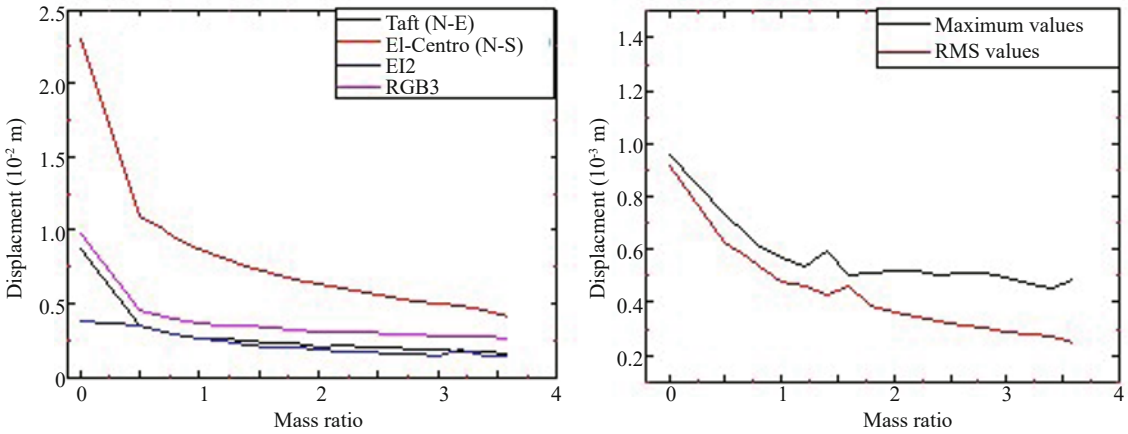

Fig. 9 Impact of mass ratio on the displacement response of MSCSS

mass ratio increases, because the sub-frames behave as vibration absorbers in this scheme. This result is expected because the effectiveness of tuned mass dampers increases with an increase in the attached mass (De Domenico and Ricciardi, 2018a; Bekdaş and Nigdeli, 2013). From *RM*=0 to 3.5, it can be seen that the acceleration and displacement gradually decrease.

7.2 Sub structural stiffness ratio (*RD*)

The sub-structural stiffness ratio is an essential parameter in controlling the mechanism of the entire structure, and which is in agreement with literature studies concerning the optimization of vibration absorbers (De Domenico *et al*., 2018, De Domenico and Ricciardi, 2018b). Hence, it should be understood clearly and analyzed adequately to improve the effectiveness of the structure under earthquake actions. To study the influence of this parameter on the control effectiveness of the entire system, the *RD* is represented as:

$$RD = \frac{K_{\text{sub}}}{K_{\text{mega}} \times N_{\text{s}}} \tag{32}$$

where K_{sub} represents the inter-floor stiffness of the substructure and is defined by Eq. (33), and K_{mega} denotes the mega-structure stiffness and is calculated from Eq. (34):

$$K_{\text{sub}} = 0.142 \times 10^{6} \times E \times I_{\text{sub}} \tag{33}$$

$$K_{\text{mega}} = \frac{3EI}{H_{\text{mega}}^{3}} \tag{34}$$

where E is the elastic modulus of the steel; I represent the moment of inertia of the mega-column; H_{mega} is the total height of the building and N_{s} is the number of the floor in one substructure.

The optimal model is analyzed under different earthquake ground motions, El-Centro (1940-NS), Taft (NE), EI2 and RGB3 earthquake waves using the fast nonlinear analysis (FNA) method and the analysis results are presented in Figs. 10 and 11, respectively, for both the maximum and root mean square RMS values of acceleration and displacement with different values of *RD*.

The results depicted in Figs. 10 and 11 show that the target response of these types of structural changes with the stiffness ratio variations and the various controlling mechanisms are seen. From Fig. 10, it is observed that the smallest acceleration responses of the building for all the earthquake waves are attained when the stiffness ratio is calculated between 0.1 – 0.4. At $RD > 0.4$ El Centro (NE) and the EI2 experience a slight increase and become stable at $RD > 0.8$. In addition, for the RMS and max values from Fig. 10 at $RD < 0.1$, the structure experiences a rapid fall in the target response (acceleration and displacement). While for $RD = 0.1$–0.4, the structure experiences minimum target response and the response slightly increases and turns to a nearly stable point at $RD > 0.8$. The variation and complex nature of MSCSS and its controlling performance with different *RM* and *RD* is shown in Fig. 12. It is revealed that for $RM = 3.5$ and $RD = 0.1$–0.4, the acceleration and displacement of the structure can be clearly decreased, as expected.

7.3 Influence of the damping ratio effect on the system

Viscous dampers are an important part of the mega-sub controlled structural system, and their parameter changes have a significant impact on structural parameters. The damping ratio of RC is also investigated in this research. The *RC* is defined by Eq. (35) as follows:

$$RC = \frac{n \times C_{\text{ms}}}{C_{\text{sub}}} \tag{35}$$

where n is the number of dampers per sub-structure,

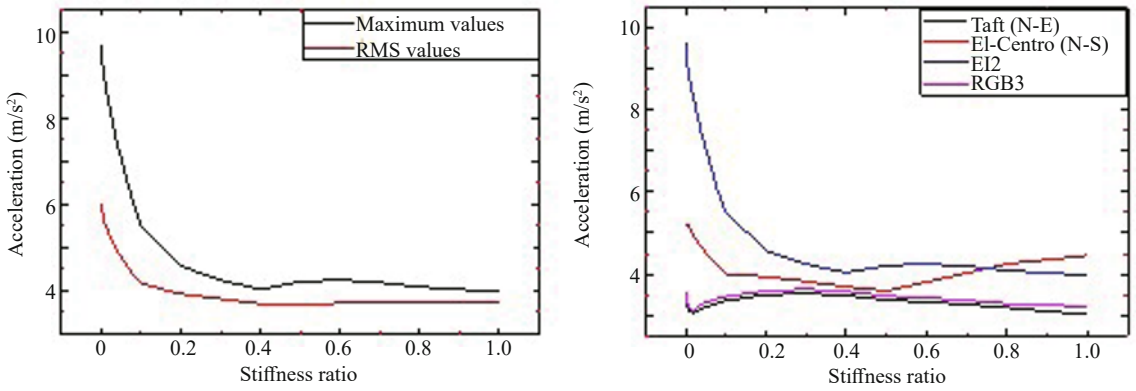

Fig. 10 Impact of stiffness ratio on the acceleration of MSCSS

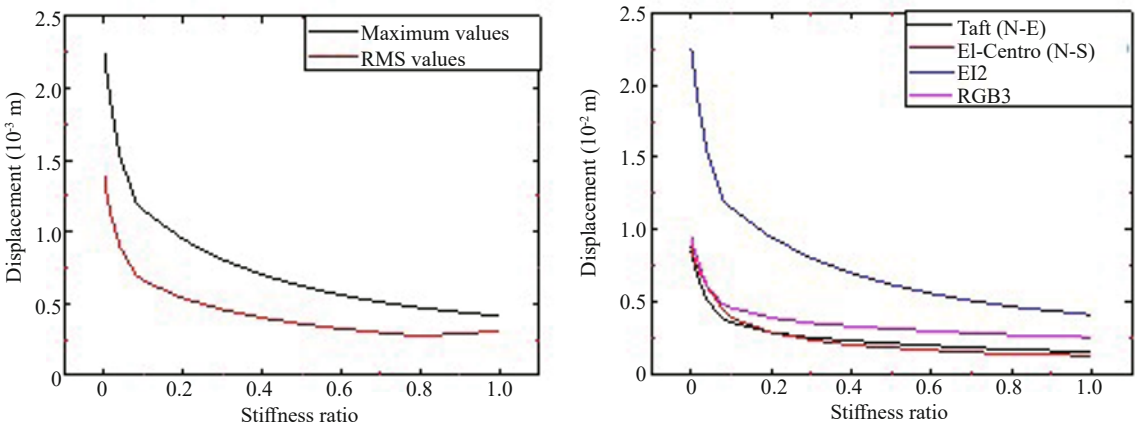

Fig. 11 Impact of stiffness ratio on displacement of MSCSS

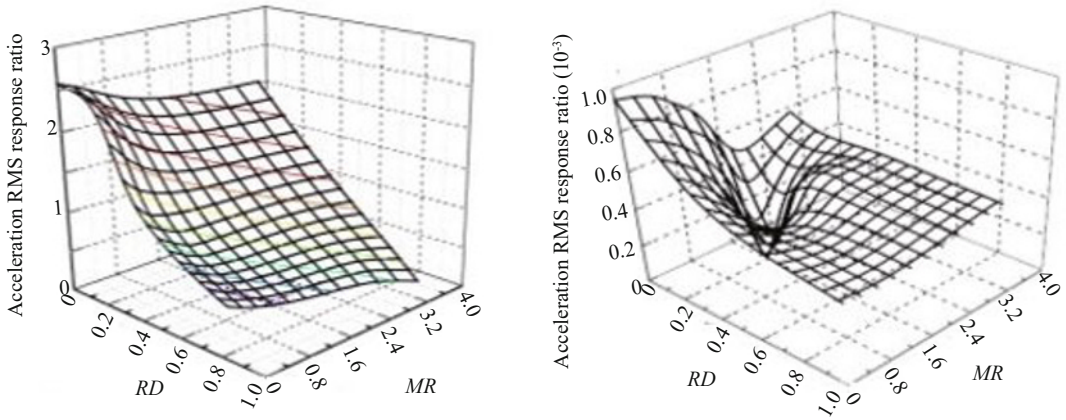

Fig. 12 RMS acceleration and displacement response at the peak level of the mega floor structure

C_{ms} is the damping of the viscous damper set between megastructure and substructure, and C_{sub} is the sub-structure story damping.

For RM = 0.7 and RD = 0.01, Model 4 (optimal model) is investigated using different values of the damping ratio (RC) and damping stiffness (K), and the analysis results demonstrate the impact of dampers on the mega sub-controlled structure system. The simulation results are compared to those of the conventional mega substructure (MSS), and the Maxwell model of the viscous damper was considered during the simulation. As seen from the control result at the top mega-floor frame, for small values of damping stiffness K and damping ratio RC, the acceleration and displacement responses of the MSCSS are higher than that of MSS. In addition, from Figs. 13 and 14, for $K = 4.0\times10^2 - K = 7.0\times10^7$, the target responses seem to be unchanged for any value of RC. While for $RC = 4.0\times10^6 - 3.0\times10^7$, the controlling effect of MSCSS increases and reaches its maximum.

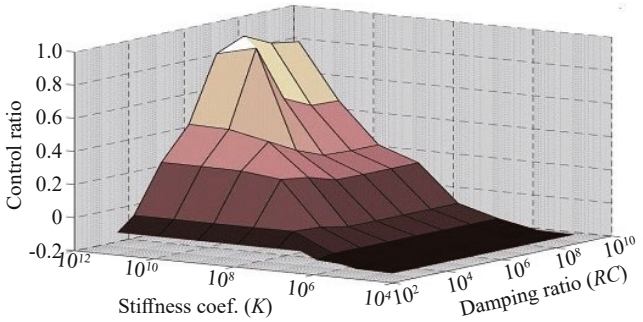

Fig. 13 Damping ratio (*RC*) Influence on acceleration response of the building for *RM* = 0.7 and *RD* = 0.01

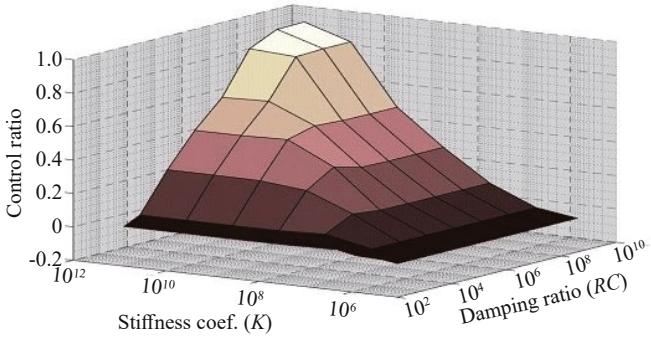

Fig. 14 Damping ratio (*RC*) Influence on displacement response of the building for *RM* = 0.7 and *RD* = 0.01

8 Conclusions

The new configuration of MSCSS proposed herein demonstrates some concepts and new ideas to further improve the performance of buildings under a strong earthquake. The performance and optimum values of the dynamic parameters of the building have been investigated.

From the numerical results, it is found that

- The results showed the extraordinary performance effectiveness of MSCSS in controlling the acceleration and displacement responses. The controlling effectiveness could be up to 42%–70% for top mega-frame structural acceleration and displacement and 20%–65% for sub-structural acceleration and displacement responses.
- Based on the dynamic parameters investigation carried out in this study, the control efficacy of the structure with varying *RD*, *RM* and *RC* is different. As such, the optimum range of the stiffness ratio *RD* with a different mass ratio *MR* is revealed in which the target responses of the MSCSS reach their optimum (minimum) values.
- When two viscous dampers are installed within the substructure of each mega-floor, the *RC* should be chosen within the 4.0×10^6 – 3.0×10^7 range and the relative stiffness ratio RD should be between 0.1–0.4. An increase in mass ratio RM will lead to greater control effectiveness of the MSCSS.
- These dynamic parameters can be used as a handy tool for structural engineering design.
- As future lines of research, inerter can be used in MSCSS as a mass amplification device in combination with vibration-absorbers. The inerter, which generates a resisting force proportional to the relative acceleration at its two terminals, can increase the inertial properties of the system to which it is attached without the need to allocate a large mass (De Domenico and Ricciardi, 2018a, 2018c; Lazar *et al*., 2014; De Domenico *et al.*, 2019a).

References

Abdulhadi M, Zhang XA, Fan B and Muhammad MS (2020a), "Design, Optimization and Nonlinear Response Control Analysis of the Mega-Sub Controlled Structural System (MSCSS) Under Earthquake Action," *Journal of Earthquake and Tsunami*, **14**(3): 2050013.

Abdulhadi M, Zhang XA, Fan and Muhammad MS (2020b), "Evaluation of Seismic Fragility Analysis of the Mega Sub-Controlled Structure System (MSCSS)," *Journal of Earthquake and Tsunami*, **14**(6): 2050025.

Amini F and Doroudi R (2010), "Control of a Building Complex with Magneto-Rheological Dampers and Tuned Mass Damper," *Structural Engineering &Mechanics,* **36**(2): 181–195.

Anwar GA and Dong Y (2020), "Seismic Resilience of Retrofitted RC Buildings," *Earthquake Engineering and Engineering Vibration*, **19**(3): 561–571.

Benoit B, Charles PL, Jean P, Patrick P (2013), "Analysis of a Damage 12-Story Frame – Wall Concrete Building During the 2010 Haiti Earthquake Part 1: Dynamic Behaviour Assessment," *Canadian Journal of Civil Engineering*, **40**(8): 791–8.

Bekdaş G and Nigdeli SM (2013), "Mass Ratio Factor for Optimum Tuned Mass Damper Strategies," *International Journal of Mechanical Sciences*, **71**: 68–84.

Byron FW and Fuller RW (1992), *Mathematics of Classical and Quantum Physic*, Dover Publication, Inc., New York, USA.

Chai W and Feng MQ (1997), "Vibration Control of Super-Tall Buildings Subjected to Wind Loads," *Int. J. Non-Linear Mechanics*, **32**(4): 657–668.

Computer and Structure Incorporated (CSI) (2014), "Integrated Software for Structural Analysis and Design, SAP 2000. V.17," Berkeley, CA, USA. http://www.csiamerica.com/sap2000

De Domenico D, Deastra P, Ricciard G, Sims ND and Wagg DJ (2019a), "Novel Fluid Inerter Based Tuned Mass Dampers for Optimized Structural Control of Base-Isolated Buildings," *Journal of the Franklin Institute*, **356**(14): 7626–7649.

De Domenico D, Impollonia N and Ricciardi G (2018), "Soil-Dependent Optimum Design of a New Passive

Vibration Control System Combining Seismic Base Isolation with Tuned Inerter Damper," *Soil Dynamics and Earthquake Engineering*, **105**: 37–53.

De Domenico D and Ricciardi G (2018a), "An Enhanced Base Isolation System Equipped with Optimal Tuned Mass Damper Inerter (TMDI)," *Earthquake Engineering & Structural Dynamics*, **47**(5): 1169–1192.

De Domenico D and Ricciardi G (2018b), "Earthquake-Resilient Design of Base-Isolated Buildings with TMD at Basement: Application to a Case Study," *Soil Dynamics and Earthquake Engineering*, **113**: 503–521.

De Domenico D and Ricciardi G (2018c), "Optimal Design and Seismic Performance of Tuned Mass Damper Inerter (TMDI) for Structures with Nonlinear Base Isolation Systems," *Earthquake Engineering & Structural Dynamics*, **47**(12): 2539–2560.

De Domenico D and Ricciardi G (2019a), "Dynamic Response of Non-Classically Damped Structures via Reduced-Order Complex Modal Analysis: Two Novel Truncation Measures," *Journal of Sound and Vibration*, **452**: 169–190.

De Domenico D and Ricciardi G (2019b), "Earthquake Protection of Structures with Nonlinear Viscous Dampers Optimized Through an Energy-Based Stochastic Approach," *Engineering Structures*, **179**: 523–539.

De Domenico D, Ricciardi G and Takewaki I (2019b), "Design Strategies of Viscous Dampers for Seismic Protection of Building Structures: A Review, *Soil Dynamics and Earthquake Engineering*, **118**: 144–165.

Diotallevi PP, Landi L and Dellavalle A (2008), "Simplified Design Methodology for Systems Equipped with Non-Linear Viscous Dampers," *The 14th World Conference on Earthquake Engineering*, Beijing, China, October.

Elghazoul AS (2002), "Over Strength and Force Reduction Factors of Multi-Story RC Buildings," *The Structural Design of Tall and Special Buildings*, **11**(5): 329–351.

Fan B, Zhang XA, Abdulhadi M and Wang ZH (2020), "Generic Optimization, Energy Analysis, and Seismic Response Study for MSCSS with Rubber Bearings," *Earthquake and Structure*, **19**(5): 347–359.

Feng MQ and Mita A (1995), "Vibration Control of Tall Buildings Using Mega-Sub Configuration," *ASCE*, *Journal of Engineering Mechanics*, **121**(10): 1082–1087.

Gabor D (1946), "Theory of Communication," *Journal of the Institution of Electrical Engineers - Part III,* **93**(26): 429–441.

GB 50011 – 2010 (2010), *Code for Seismic Design of the Buildings*, National Standard of the People Republic of China, Ministry of Housing and Urban-Rural Development of the People Republic of China, Beijing, China.

Hwang JS, Lin WC and Wu NJ (2013), "Comparison of Distribution Methods for Viscous Damping Coefficients to Buildings, *Structure and Infrastructure Engineering*, **9**(1): 28–41.

Khan MA, Akhtar K, Ahmad N, Shah F and Khattak N (2020), "Vibration Analysis of Damaged and Undamaged Steel Structure Systems: Cantilever Column and Frame," *Earthquake Engineering and Engineering Vibration*, **19**(3): 725–737.

Kim HS and Lee KH (2010), "Fuzzy Hybrid Control of a Wind-Excited Tall Building," *Structural Engineering & Mechanics*, **36**(3): 381–399.

Lan Z, Fang L and Wang X (2002), "Multi-Functional Shock Absorption System of RC Mega Structure," *Industrial construction*, **32**(2): 1–4.

Lazar IF, Neild SA and Wagg DJ (2014), "Using an Inerter-Based Device for Structural Vibration Suppression," *Earthquake Engineering & Structural Dynamics*, **43**(8): 1129–1147.

Lian YD, Zhang XA and Cherry S (2007), "Damping Characteristics of Friction Damped Braced Frame and Its Effectiveness in the Mega-Sub Controlled Structure System," *Earthquake Engineering and Engineering Vibration*, **6**(2): 171–181.

Murat S, Palermo D, Ahmad G, Denis M, Simpson R, Perry A, Robert T, Carlos V and Hanping H (2013), "Performance of Steel Building and Nonstructural Elements During the 2010 Maule (Chile) Earthquake," *Canadian Journal of Civil Engineering*, **40**(8): 722–734.

Ndemanou BP, Metsebo BR, Nbendjo N and Woafo P (2014) "Dynamics and Magneto Rheological Control of Vibration of Cantilever Timoshenko Beam Under Earthquake Load," *Nonlinear Dyn*., **78**(1): 163–171.

Vona M and Mastroberti M (2018), "Estimation of the Behavior Factor of Existing RC-MRF Buildings," *Earthquake Engineering and Engineering Vibration*, **17**(1): 191–204.

Whittle JK, Williams MS, Karavasilis TL and Blakeborough A (2012), "A Comparison of Viscous Damper Placement Methods for Improving Seismic Building Design," *Journal of Earthquake Engineering*, **16**(4): 540–560.

Yang C, Xie L, Li A, Zeng D, Jia J, Chen X and Chen M (2020), "Resilience-Based Retrofitting of Existing Urban RC-Frame Buildings Using Seismic Isolation," *Earthquake Engineering and Engineering Vibration*, **19**(4): 839–853.

Zhang JL, Zhang XA and Jiang JS (2004), "Dynamic Analysis of a Vibration Absorption System of a Mega Frame via Considering the Influence of Substructure," *Proceeding of the Eighth International Symposia on Structural Engineering for Young Expert*, Guangzhou, China. (in Chinese)

Zhang XA, Qin XJ, Cherry S, Lian YD, Zhang JL and Jiang JS (2009), "A New Proposed Passive Mega-Sub

Controlled Structure and Response Control," *Journal of Earthquake Engineering*, **13**(2): 252–274.

Zhang XA, Wang D and Jiang JS (2005a), "The Controlling Mechanism and the Controlling Effectiveness of Passive Mega-Sub-Controlled Frame Subjected to Random Wind Loads," *Journal of Sound and Vibration*, **283**: 543–560.

Zhang XA, Zhang JL, Wang D and Jiang JS (2005b), "Controlling Characteristics of Passive Mega-Sub Controlled Frame Substructure to Random Wind Loads," *Journal of Engineering Mechanics*, *ASCE*, **131**(10): 1046–1055.

Zhou FL and Tan P (2018), "Recent Progress and Application on Seismic Isolation Energy Dissipation and Control for Structures in China," *Earthquake Engineering and Engineering Vibration*, **17**(1): 19–27.

Appendix A Parameters assemblies of the system dynamic equation

A1 Assembling the stiffness matrix *K*

The matrix $\boldsymbol{K}_{si}$ from Eq. (4) can be expressed as;

$$\boldsymbol{K}_{si}=\begin{bmatrix} K_{i,1}+K_{i,2} & -K_{i,2} & 0 & 0 & \cdots & 0 \\ -K_{i,2} & K_{i,2}+K_{i,3} & -K_{i,3} & 0 & \cdots & 0 \\ \vdots & \vdots & \ddots & \ddots & \ddots & \vdots \\ 0 & 0 & 0 & -K_{i,nz-1} & K_{i,nz-1}+K_{i,nz} & -K_{i,nz} \\ \vdots & \vdots & \vdots & \vdots & \vdots & \vdots \\ 0 & 0 & \cdots & 0 & -K_{i,nz} & K_{i,nz} \end{bmatrix}_{nz\times nz}$$

where $K_{i,1}$ (i = 1, 2,….., n_1) is the shear stiffness value of the ith substructure. The matrix $\boldsymbol{K}_c$ in Eq. (3) is the parameter connecting the mega-structure and the sub-structures and has $n \times n_1 n_z$ matrix elements.

$$\boldsymbol{K}_c=\begin{array}{c} \\ 1 \\ 2 \\ \vdots \\ \vdots \\ \vdots \\ i \\ \vdots \\ n_1 \\ \vdots \\ \vdots \\ \vdots \\ \vdots \\ n \end{array}\begin{bmatrix} 1 & 2 & \cdots & n_z+1 & \cdots & 2n_z+1 & \cdots & (i-1)n_z+1 & \cdots & (n_1-1)n_z+1 & \cdots & n_1 n_z \\ -K_{1,1} & 0 & \cdots & 0 & \cdots & 0 & \cdots & 0 & \cdots & 0 & \cdots & 0 \\ 0 & 0 & \cdots & 0 & \cdots & 0 & \cdots & 0 & \cdots & 0 & \cdots & 0 \\ \vdots & \vdots & \vdots & -K_{2,1} & \vdots & \vdots & \vdots & \vdots & \vdots & \vdots & \vdots & \vdots \\ 0 & 0 & \cdots & 0 & \cdots & -K_{3,1} & \cdots & 0 & \cdots & 0 & \cdots & 0 \\ 0 & 0 & \cdots & 0 & \cdots & \cdots & \cdots & -K_{i,1} & \cdots & 0 & \cdots & 0 \\ \vdots & \vdots & \vdots & \vdots & \vdots & \vdots & \vdots & \vdots & \vdots & \vdots & \vdots & \vdots \\ 0 & 0 & \cdots & 0 & \cdots & 0 & \cdots & 0 & \cdots & -K_{n,1} & \cdots & 0 \\ 0 & 0 & \cdots & 0 & \cdots & 0 & \cdots & 0 & \cdots & 0 & \cdots & 0 \\ \vdots & \vdots & \vdots & \vdots & \vdots & \vdots & \vdots & \vdots & \vdots & \vdots & \vdots & \vdots \\ 0 & 0 & \cdots & 0 & \cdots & 0 & \cdots & 0 & \cdots & 0 & \cdots & 0 \\ 0 & 0 & \cdots & 0 & \cdots & 0 & \cdots & 0 & \cdots & 0 & \cdots & 0 \\ 0 & 0 & \cdots & 0 & \cdots & 0 & \cdots & 0 & \cdots & 0 & \cdots & 0 \end{bmatrix}_{n_1 n_z}$$

In addition, the sub matrix $\boldsymbol{K}_p + \boldsymbol{K}_{s,diag}$ of Eq. (3) can be assembled in the following form:

$$\boldsymbol{K}_{\mathrm{P}}+\boldsymbol{K}_{\mathrm{s,diag}}=\begin{bmatrix} K_{\mathrm{P1},1}+K_{1,1} & K_{\mathrm{P1},2} & \cdots & K_{\mathrm{P1},i} & \cdots & K_{\mathrm{P1},n-1} & K_{\mathrm{P1},n} \\ K_{\mathrm{P2},1} & K_{\mathrm{P2},2}+K_{2,1} & \cdots & K_{\mathrm{P2},i} & \cdots & K_{\mathrm{P2},n-1} & K_{\mathrm{P2},n} \\ \vdots & \vdots & \ddots & \vdots & \ddots & \vdots & \vdots \\ K_{\mathrm{P}i,1} & K_{\mathrm{P}i,2} & \cdots & K_{\mathrm{P}i,i}+K_{i,1} & \cdots & K_{\mathrm{P}i,n-1} & K_{\mathrm{P}i,n} \\ \vdots & \vdots & \ddots & \vdots & \ddots & \vdots & \vdots \\ K_{\mathrm{P}n-1,1} & K_{\mathrm{P}n-1,2} & \cdots & K_{\mathrm{P}n-1,i} & \cdots & K_{\mathrm{P}n-1,n-1}+K_{n1,1} & K_{\mathrm{P}n-1,n} \\ K_{\mathrm{P}n,1} & K_{\mathrm{P}n,2} & \cdots & K_{\mathrm{P}n,i} & \cdots & K_{\mathrm{P}n,n-1} & K_{\mathrm{P}n,n} \end{bmatrix}_{n\times n}$$

where $\boldsymbol{K}_{\mathrm{p}i,j}$ (i, j = 1, 2, 3, ……., n) is the item of the stiffness matrix $\boldsymbol{K}_{\mathrm{p}}$ of the mega-structure, and $\boldsymbol{K}_{i,l}$ (i =1, 2, 3, …..…., n_1) is the shear stiffness value of the ith sub-structure.

A2 Assembling the damping matrix *C*

Damping matrix $\boldsymbol{C}$ is assembled the same way as stiffness matrix $\boldsymbol{K}$; therefore, the submatrix from Eqs. (5) and (6) can be expressed as:

$$\boldsymbol{C}_{si}=\begin{bmatrix} C_{i,1}+C_{i,2} & -C_{i,2} & 0 & 0 & \cdots & 0 \\ -C_{i,2} & C_{i,2}+C_{i,3} & -C_{i,3} & 0 & \cdots & 0 \\ \vdots & \vdots & \ddots & \ddots & \ddots & \vdots \\ 0 & 0 & 0 & -C_{i,nz-1} & C_{i,nz-1}+C_{i,nz} & -C_{i,nz} \\ \vdots & \vdots & \vdots & \vdots & \vdots & \vdots \\ 0 & 0 & \cdots & 0 & -C_{i,nz} & C_{i,nz} \end{bmatrix}_{nz\times nz}$$

$$\boldsymbol{C}_{\mathrm{c}}=\begin{array}{c} \\ 1 \\ 2 \\ \vdots \\ \vdots \\ \vdots \\ i \\ \vdots \\ n_1 \\ \vdots \\ \vdots \\ \vdots \\ \vdots \\ \vdots \\ n \end{array}\begin{bmatrix} 1 & 2 & \cdots & n_z+1 & \cdots & 2n_z+1 & \cdots & (i-1)n_z+1 & \cdots & (n_1-1)n_z+1 & \cdots & n_1n_z \\ -C_{1,1} & 0 & \cdots & 0 & \cdots & 0 & \cdots & 0 & \cdots & 0 & \cdots & 0 \\ 0 & 0 & \cdots & 0 & \cdots & 0 & \cdots & 0 & \cdots & 0 & \cdots & 0 \\ \vdots & \vdots & \vdots & -C_{2,1} & \vdots & \vdots & \vdots & \vdots & \vdots & \vdots & \vdots & \vdots \\ 0 & 0 & \cdots & 0 & \cdots & -C_{3,1} & \cdots & 0 & \cdots & 0 & \cdots & 0 \\ 0 & 0 & \cdots & 0 & \cdots & \cdots & \cdots & -C_{i,1} & \cdots & 0 & \cdots & 0 \\ \vdots & \vdots & \vdots & \vdots & \vdots & \vdots & \vdots & \vdots & \vdots & \vdots & \vdots & \vdots \\ 0 & 0 & \cdots & 0 & \cdots & 0 & \cdots & 0 & \cdots & -C_{n,1} & \cdots & 0 \\ 0 & 0 & \cdots & 0 & \cdots & 0 & \cdots & 0 & \cdots & 0 & \cdots & 0 \\ \vdots & \vdots & \vdots & \vdots & \vdots & \vdots & \vdots & \vdots & \vdots & \vdots & \vdots & \vdots \\ 0 & 0 & \cdots & 0 & \cdots & 0 & \cdots & 0 & \cdots & 0 & \cdots & 0 \\ 0 & 0 & \cdots & 0 & \cdots & 0 & \cdots & 0 & \cdots & 0 & \cdots & 0 \\ 0 & 0 & \cdots & 0 & \cdots & 0 & \cdots & 0 & \cdots & 0 & \cdots & 0 \end{bmatrix}_{n_1n_z}$$

$$\boldsymbol{C}_{\mathrm{P}}+\boldsymbol{C}_{\mathrm{s,diag}}=\begin{bmatrix} C_{\mathrm{P1},1}+C_{1,1} & C_{\mathrm{P1},2} & \cdots & C_{\mathrm{P1},i} & \cdots & C_{\mathrm{P1},n-1} & C_{\mathrm{P1},n} \\ C_{\mathrm{P2},1} & C_{\mathrm{P2},2}+C_{2,1} & \cdots & C_{\mathrm{P2},i} & \cdots & C_{\mathrm{P2},n-1} & C_{\mathrm{P2},n} \\ \vdots & \vdots & \ddots & \vdots & \ddots & \vdots & \vdots \\ C_{\mathrm{P}i,1} & C_{\mathrm{P}i,2} & \cdots & C_{\mathrm{P}i,i}+C_{i,1} & \cdots & C_{\mathrm{P}i,n-1} & C_{\mathrm{P}i,n} \\ \vdots & \vdots & \ddots & \vdots & \ddots & \vdots & \vdots \\ C_{\mathrm{P}n-1,1} & C_{\mathrm{P}n-1,2} & \cdots & C_{\mathrm{P}n-1,i} & \cdots & C_{\mathrm{P}n-1,n-1}+C_{n1,1} & C_{\mathrm{P}n-1,n} \\ C_{\mathrm{P}n,1} & C_{\mathrm{P}n,2} & \cdots & C_{\mathrm{P}n,i} & \cdots & C_{\mathrm{P}n,n-1} & C_{\mathrm{P}n,n} \end{bmatrix}_{n\times n}$$

A3 Load vector provided by damping device and rubber bearings

The load vector $\boldsymbol{p}(t)$ from Eq. (1) can be expressed as:

$$\begin{aligned}
&\boldsymbol{p}_{(t),i} = adc(u_{i,n_z} - u_{\mathrm{p},i}) + rbk(u_{i,n_z} - u_{\mathrm{p},i}) \\
&i = 2, 3, ..., n-1 \\
&\boldsymbol{p}_{(t),n} = adc(u_{n,n_z} - u_{\mathrm{p},n}) + rbk(u_{n,n_z} - u_{\mathrm{p},n})
\end{aligned}$$

where adc is the damping value of the damping device, and rbk is the shear stiffness of the rubber bearing.